High Power Laser Science and Engineering, (2024), Vol. 12, e77, 7 pages.
doi:10.1017/hpl.2024.51

HIGH POWER LASER SCIENCE AND ENGINEERING

RESEARCH ARTICLE

Improved method to optimize the phase jump of multiple exposure-tiled gratings

Xinhui Ding[1,2], Hui Yu[1,2], Dawei Li[1], Junyong Zhang[1], Li Wang[1], Qiong Zhou[1], and Xingqiang Lu[1]

[1]*National Laboratory on High Power Lasers and Physics, Shanghai Institute of Optics and Fine Mechanics, Chinese Academy of Sciences, Shanghai, China*

[2]*University of Chinese Academy of Sciences, Beijing, China*

(Received 15 May 2024; revised 5 July 2024; accepted 8 August 2024)

Abstract

Large-aperture gratings have significant applications in inertial confinement fusion, immersion lithography manufacturing and astronomical observation. Currently, it is challenging and expensive to manufacture sizable monolithic gratings. Therefore, tiled multiple small-aperture gratings are preferred. In this study, the impact of seam phase discontinuity on the modulation of the laser beam field was explored based on the measurement results of the Shenguang-II laser large-aperture multi-exposure-tiled grating. An innovative method for accurately calculating the phase jump of multi-exposure-tiled grating seams was proposed. An intensive electromagnetic field analysis was performed by applying rigorous coupled-wave analysis to a reasonably constructed micrometer-level periodic grating seam structure, and the phase jump appearing in millimeter-scale seams of large-aperture tiled gratings was obtained accurately.

Keywords: large-aperture grating; tiled grating; phase distribution; rigorous coupled-wave analysis

1. Introduction

Large-scale diffraction gratings are core optical components used in immersion lithography manufacturing[1], high-power lasers[2,3] and astronomical observations[4]. The increase in the aperture size of astronomical telescopes and the enhancement of laser pulse power to the petawatt (10^{15} W) level have propelled a gradual increase in the demand for larger gratings[5]. The Lawrence Livermore National Laboratory (LLNL) has fabricated holographic gratings with a diameter of up to 940 mm using single-exposure techniques[6]. However, for even larger gratings, costly monolithic large-scale grating manufacturing techniques or methods involving the assembly of multiple smaller gratings, such as the 1.41 m × 0.43 m grating used in the OMEGA EP pulse compressor, are required. The latter involves the assembly of three smaller gratings (0.47 m × 0.43 m) through adjustable mechanical structures[7].

Grating assembly methods involve mechanical assembly and exposure tiling[8]. Mechanical assembly involves using mechanical devices to fix subgratings while continuously monitoring and adjusting their relative positions to ensure phase coherence. However, owing to the influence of mechanical adjustment structures[7,9], mechanically assembled gratings exhibit errors over time, including the line density error Δd and rotational and translational errors θ_x, θ_y, θ_z, Δx and Δz. In contrast, exposure tiling involves exposing multiple regions of the substrate several times to produce a single large grating, such as the 1025 mm × 350 mm grating used in the Shenguang-II (SG-II) laser. Precise substrate movement can control errors such as θ_x, θ_y, θ_z, Δx and Δz at lower levels[10], resulting in higher manufacturing precision and spectral resolution. Therefore, multi-exposure-tiled gratings are commonly employed in applications with stringent grating requirements, such as high-power lasers.

Owing to the precorrection of out-of-plane errors in exposure tiling, it is crucial to study the effects of the seams generated during the tiling process. Rigorous coupled-wave analysis (RCWA) is an accurate method for calculating the optical field of gratings and the phase distribution[11]. However, RCWA calculations are based on grating periods and require periodic structure compositions from the grating lines[12]. Owing to the difference in orders of magnitude between the actual seam width and the grating period, directly applying RCWA for intensive electromagnetic field analysis of tiled gratings is impractical. Therefore, a novel wavelength- or subwavelength-scale calculation method is required.

Correspondence to: X. Lu, National Laboratory on High Power Lasers and Physics, Shanghai Institute of Optics and Fine Mechanics, Chinese Academy of Sciences, Qinghe Rd. No. 390, Shanghai 201800, China. Email: xingqianglu@siom.ac.cn

Based on the characteristics of RCWA, this study proposed a method to equivalently model millimeter-scale seam structures in meter-scale gratings using periodic structures at the wavelength scale for the first time. This study presents the characteristics of the exposure-tiled gratings used in the SG-II laser, illustrating the influence of the seam phase jump on the optical field distribution. Subsequently, we introduce an RCWA-based calculation method to analyze the characteristics of exposure-tiled grating seams. Finally, the feasibility of applying this algorithm, which has significant implications for the fabrication of various multi-exposure-tiled gratings, is analyzed.

2. Phase jump in large-aperture tiled gratings

2.1. Phase jump in the SG-II compression chamber

As illustrated in Figure 1, the SG-II compression chamber is constructed using four large-aperture gratings. The size of these gratings can reach up to 1025 mm × 350 mm; therefore, it is not only difficult but also costly to make them monolithic. Recently, the SG-II upgraded laser facility created a large-aperture grating using exposure tiling by etching a subgrating, moving the grating substrate precisely and etching a second subgrating in the adjacent area.

The surface profile of the first exposure-tiled grating (G1 in Figure 1) in the SG-II compression chamber was obtained using an interferometer, as shown in Figure 2. A consistent relative 0.15λ phase jump was observed across the entire tiled grating, which has a width of 5 mm. This deficit during the exposure-tiling process inevitably leads to modulation.

2.2. Modulation caused by phase jump

It has been observed that the phase jump that appears in exposure-tiled gratings significantly affects the field of the subsequent component in the path[13]. Figure 3 illustrates the effect of the phase jump of G1 on the field characteristics of G2, G3 and G4 under the condition of a 0.15λ phase jump across a 5-mm-width seam, where G1 is an exposure-tiled ideal grating and the incident beam is a super-Gaussian 350-mm-wide square, ideal plane wave.

The phase discontinuity in G1 induces an intensity modulation nearly twice as high (1.89 times higher). Because the G4 grating in the compression chamber serves as the final compression stage of the laser pulses, such high-intensity modulation may lead to severe damage to the last grating[14].

In this part, only diffraction theory is applied to analyze the modulation caused by the phase jump. To determine the influence of seam characteristics in manufacturing tiled gratings, rigorous electromagnetic field calculations are essential, which ensures that seam modulation caused by the phase distribution remains acceptable and guides the fabrication of large-aperture tiled gratings.

3. Improved method

3.1. Limitations of the legacy rigorous calculation method

RCWA has been used for the rigorous electromagnetic field analysis of periodic structures at the scale of wavelengths and subwavelengths since it was first employed in the analysis of planar gratings and relief structure gratings[15,16]. Its principle involves transforming Maxwell's equations into coupled expressions of characteristic functions within the region of gratings and then applying boundary conditions at the interfaces of the grating and surrounding media to solve for diffraction efficiency and field distribution.

In the calculations, the dielectric index distribution of the grating groove must first be expanded into a Fourier series as follows:

$$\varepsilon(x) = \sum_h e_h \exp\left(\mathrm{j}\frac{2\pi}{\Lambda}hx\right). \tag{1}$$

Here, Λ is the period of the periodic structure, which is generally at the wavelength or subwavelength level; the index h represents the hth order of expansion for the dielectric constant within the grating region and e_h is the expansion coefficient. The difference in the expansion coefficient represents the morphology, etching depth and other information of different gratings, satisfying the following:

$$e_h = \frac{1}{\Lambda}\int_0^{\Lambda} \varepsilon(x)\ \exp\left(-\mathrm{j}\frac{2\pi}{\Lambda}hx\right)\mathrm{d}x. \tag{2}$$

When the grating has a simple periodic groove structure, the expansion order h is low. However, for exposure-tiled gratings, such as the gratings in the SG-II compression chamber, with seam widths of 5 mm, there is a difference of four orders of magnitude compared to the grating period of 574 nm, as illustrated in Figure 4. When applying legacy

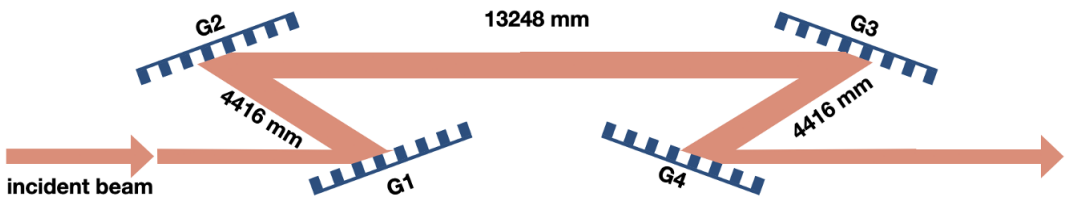

Figure 1. Layout of large-aperture tiled gratings in the SG-II compression chamber.

https://doi.org/10.1017/hpl.2024.51 Published online by Cambridge University Press

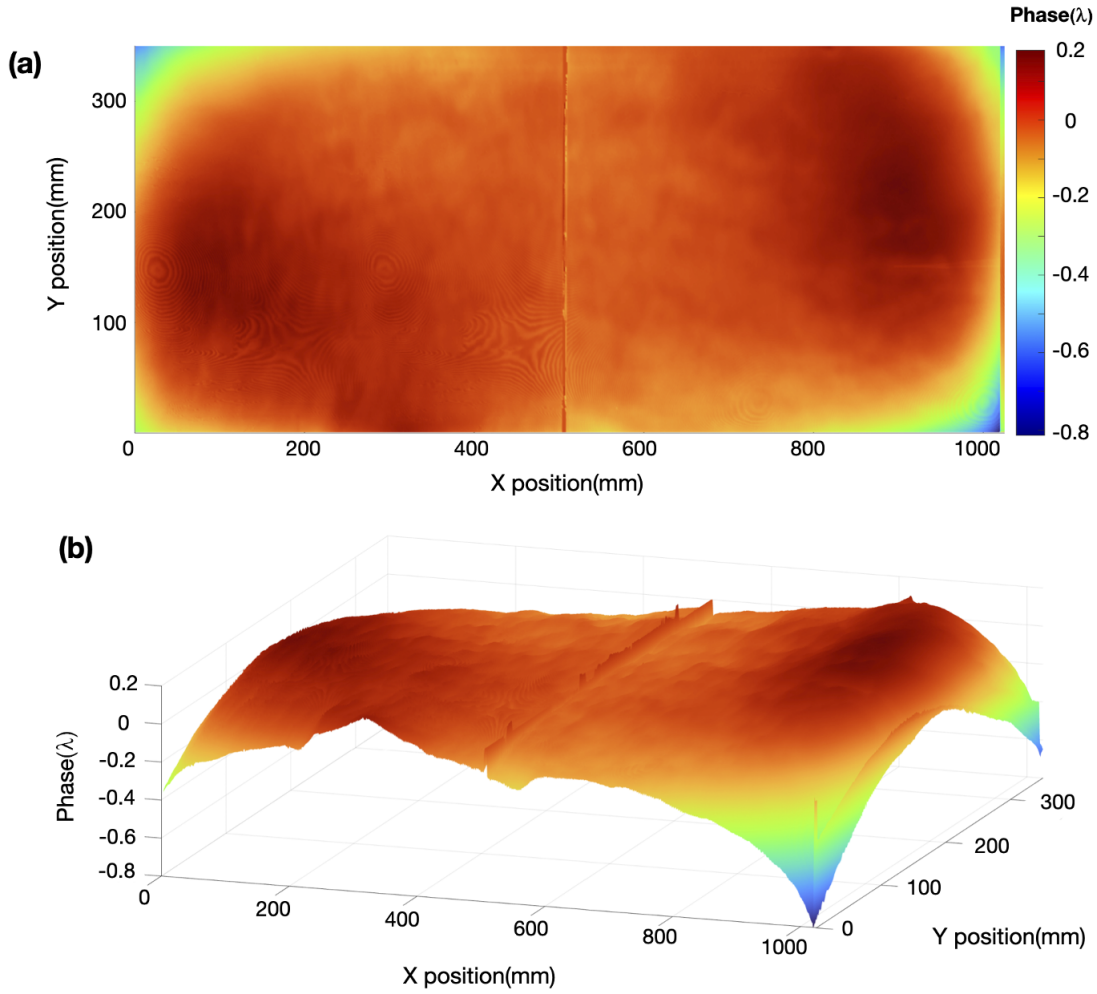

Figure 2. Wavefront of the first SG-II grating in the compression chamber observed via an interferometer. (a) Orthogonal perspective and (b) oblique perspective.

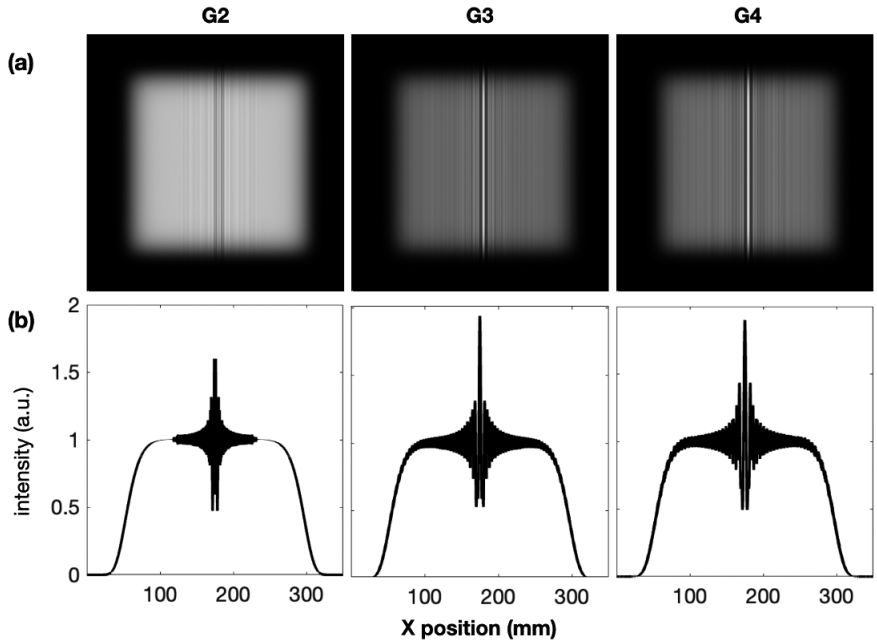

Figure 3. (a) Modulation on G2, G3 and G4 in the SG-II compressor chamber induced by tiled grating G1 with a 0.15λ phase jump and (b) one-dimensional cross section of the G2, G3 and G4 output beam.

https://doi.org/10.1017/hpl.2024.51 Published online by Cambridge University Press

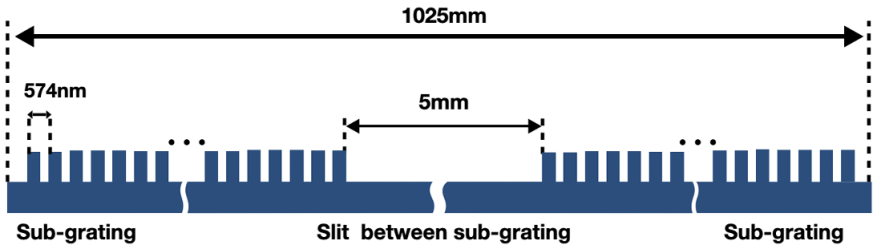

Figure 4. Illustration of a large-aperture tiled grating seam in the SG-II compression chamber.

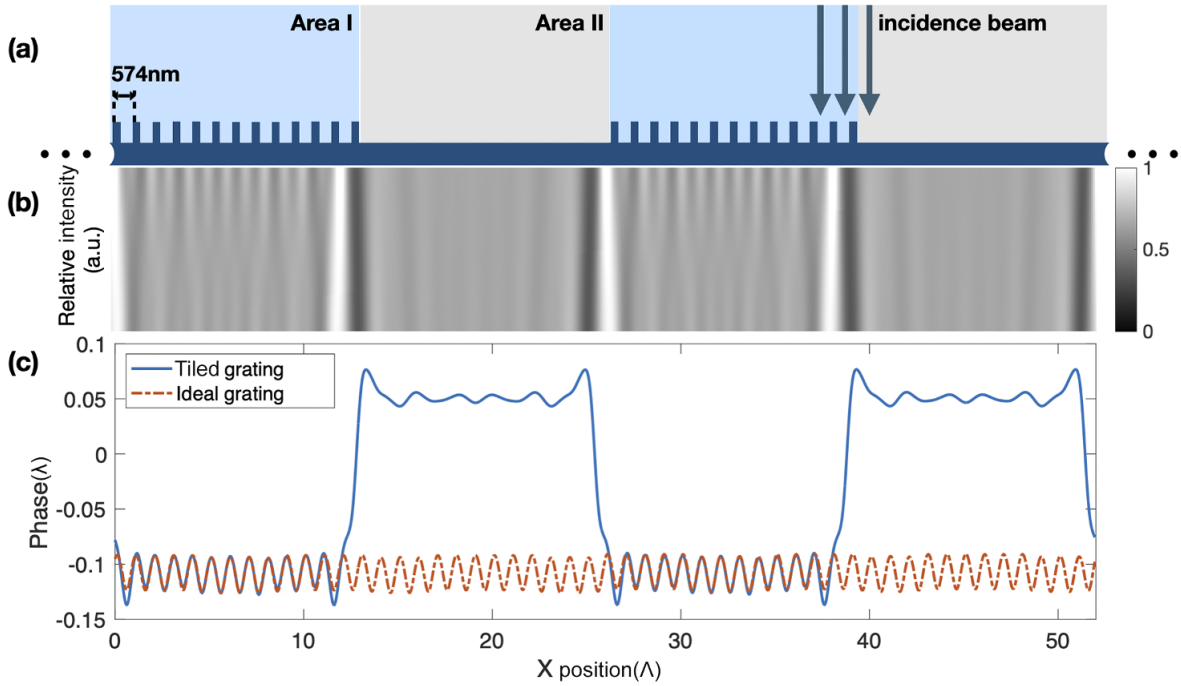

Figure 5. (a) Simplified quartz tiled grating, (b) normal incidence beam transmission field (normalized intensity) and (c) phase distribution of tiled and monolithic gratings.

RCWA to calculate tiled gratings, the expansion order is high, resulting in a vast matrix for calculation that cannot be feasibly computed.

Another method for analyzing structures, such as metasurfaces[17,18] and grating electromagnetic fields, is the finite difference time domain (FDTD) method, the accuracy of which depends on the size of the space and time grids during calculation. Considering the grating structure has a subwavelength scale, the space and time grid should be small, which incurs more computational resources. This is the consequence of applying the FDTD method to the electromagnetic field analysis of a meter-scale tiled grating, that is, an unrealizable computational resource. Therefore, certain approximations must be made to calculate the electromagnetic field characteristics of tiled gratings.

3.2. Improved RCWA for rigorous calculation of tiled gratings

To utilize RCWA of tiled gratings, a periodic quartz structure was designed in this study, as illustrated in Figure 5(a). Each period consisted of two areas. The first area comprised a series of groove structures with a period of 574 nm, consistent with the actual grating in SG-II. The other area represented air gaps without grating structures and served as a substitute for the seams in the tiled grating. Both areas had the same width of 13 times the groove period. The results of the field and phase distribution analysis conducted using RCWA in this periodic quartz structure are shown in Figures 5(b) and 5(c). Figure 5(b) illustrates the distribution of its outgoing field, and Figure 5(c) depicts the distribution of its outgoing field phase.

The solid blue line in Figure 5(c) represents the phase distribution of the constructed periodic quartz structure, and the dashed red line represents the phase distribution of an ideal monolithic quartz grating. At the center of Area I, the solid blue line is fitted with the red dashed line, indicating that in Area I, the phase distribution of the periodic quartz structure designed in this study perfectly matched the phase distribution of the ideal grating. Therefore, in Area I, the field and phase distributions at the center of this periodic

https://doi.org/10.1017/hpl.2024.51 Published online by Cambridge University Press

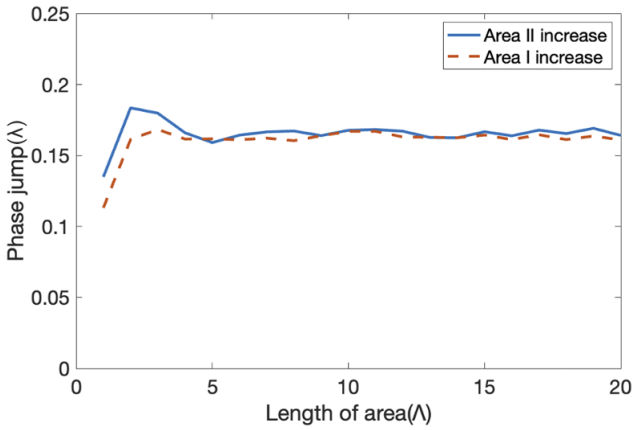

Figure 6. Phase jump with growing area width.

structure can be used to replace the ideal monolithic grating with no seam. In addition, the field and phase distributions at the grating seam can be studied using the periods at the boundary between Areas I and II, and the phase jump between the central parts of Areas I and II can be analyzed to study the phase variation of large-scale tiled grating seams. This approach circumvents the problem of a lack of periodicity in the layout of large-aperture tiled gratings, making them suitable for RCWA.

3.3. Phase jump in tiled gratings

The results in Figure 5(c) indicate a distinct and stable phase difference δ between the transmission fields of the tiled and monolithic gratings in Area II. This phase jump is defined as follows:

$$\delta = \phi_s - \phi_l, \tag{3}$$

where ϕ_l represents the phase of the monolithic grating (dashed red line) and ϕ_s corresponds to the phase at the seams of the tiled grating (solid blue line). In Figure 6, the solid blue line represents the phase difference calculated by maintaining the 13 periods constant in Area I and varying the width of Area II, whereas the dashed red line represents the phase difference calculated by maintaining the 13 periods constant in Area II and varying the width of Area I. As the widths of Areas I and II increase, the calculated phase jump tends to stabilize when the width exceeds 10Λ. The area width exceeding the 20Λ finite number of periods (FNP) grating system was studied by Wu and Glytsis in 2002[19]. When the FNP had more than 20 grooves, the result converged to the value predicted in infinite gratings (in this study, the phase jump remained stable when the length of the area extended). Therefore, it is feasible to use this periodic structure to analyze tiled gratings. To ensure computational stability, this study conducted calculations and analysis using Areas I and II, each with a width of 13Λ.

4. Application

This improved method for calculating the grating seams can be applied to various types of gratings. This study applied this method to two types of gratings: a gold-coated grating used for spectral beam combination[20] and a multilayer dielectric grating (MDG) with a higher damage threshold[21]. The gold-coated reflective grating is composed of a gold film etched onto fused quartz, whereas the MDG consists of a stack of high- and low-refractive-index material (H2L)9H3L film series deposited on a quartz substrate[22], which was the structure of gratings in the SG-II compressor chamber. The structures of these gratings are shown in Figures 7(a) and 7(b), respectively.

By constructing the period structure in this study, the phase jumps of the tiled gratings formed by the two types of grating structures were calculated. The phase jumps in the seams of these two types of tiled gratings are shown in Figure 8.

For structures with the same groove density, etching depth and period, the seams of gold-coated tiled gratings exhibit a more pronounced phase jump than those of multilayer dielectric tiled gratings. To further investigate the impact of the seam on the phases of both types of gratings, the phase jump was calculated for different etching treatments

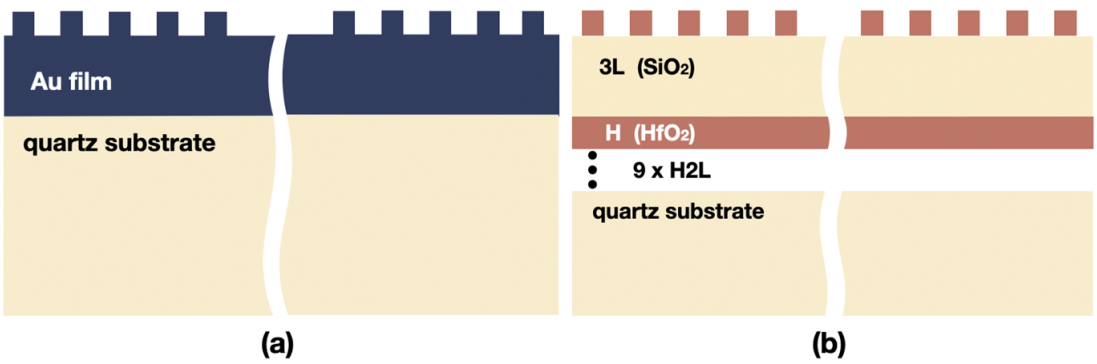

Figure 7. Structure of typical gratings used in the study: (a) Au-coated grating and (b) multilayer dielectric grating.

https://doi.org/10.1017/hpl.2024.51 Published online by Cambridge University Press

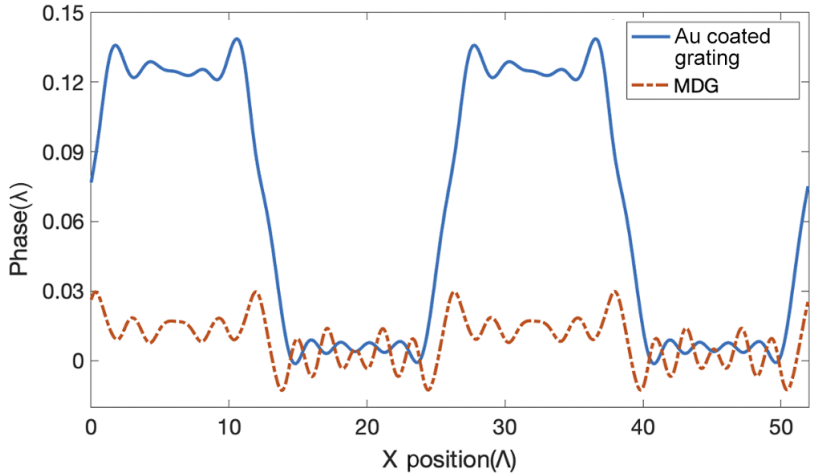

Figure 8. Phase distribution in the seams of the tiled Au-coated and tiled multilayer dielectric gratings.

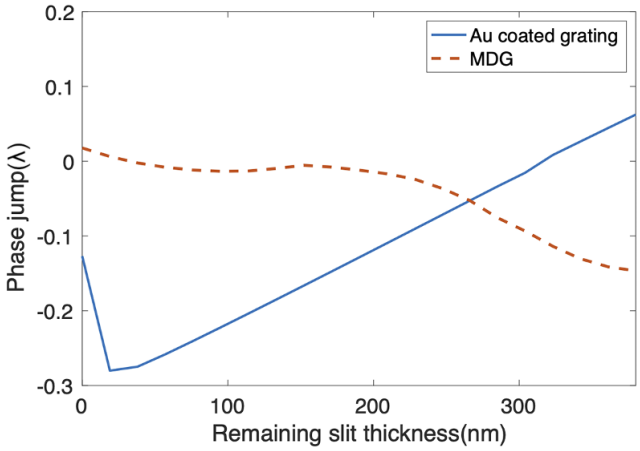

Figure 9. Phase jump in the tiled grating seams affected by the remaining slit thickness, where a 0-nm remaining thickness indicates that the seam was fully etched, whereas 380 nm implies no etching was applied to the seams.

of the tiled grating seams. Different etching depths of seams with a high refractive index were calculated. The influence of seam treatments on the phase jump is illustrated in Figure 9 (both tiled gratings in this study had the same parameters as gratings in the SG-II compression chamber, 380-nm depth and 574-nm period grooves). The end of the dashed red line in Figure 9 was the structure measured by the interferometer in Figure 2, which shows the same relative 0.15λ phase jump measured. The results indicate that a sharper and more pronounced phase jump occurred in the gold-coated tiled gratings when the remaining thickness of the high-refractive-index material in the seams was changed.

To ensure the consistency of the tiled grating phase, the seams of the tiled MDG should ensure complete etching of the high-refractive-index materials. When incomplete etching occurs at the seams of the tiled MDG, a significant phase jump occurs. Conversely, for gold-coated tiled gratings, etching should not be applied to the high-refractive-index material of the seams to ensure smoother phase continuity. In addition, the impact of the seam treatment on the phase jump of the gold-coated gratings is more significant. An MDG is recommended for manufacturing large-aperture tiled gratings to ensure the consistency of the phase in the outgoing field from the gratings. The seams of the tiled MDG should be etched close to the substrate level to ensure phase continuity.

5. Conclusion

In this study, the layout of the compression chamber in the SG-II petawatt laser was combined to demonstrate a significant degradation in beam quality caused by the phase jump in exposure-tiled grating seams. To address the inability to rigorously calculate the phase jump in exposure-tiled grating seams, an improved calculation method based on RCWA was proposed. This method uses a finite period of grating grooves and a micrometer-level grating gap to form a periodic structure, which is used to represent the large-aperture gratings and millimeter-scale width of the seams in exposure-tiled gratings. Therefore, high-precision phase computing can be achieved using minimal resources. The feasibility of this method, the number of grooves used to represent large-aperture gratings and the selection of micrometer-level gaps used to represent millimeter-scale grating seams were systematically studied. The principles of the construction parameters have been provided.

The phase jump of both the tiled gold-coated grating and tiled MDG was further studied, ensuring the phase continuity of these types of grating seams. This method can be applied to various types of tiled gratings and can be used to conduct further studies on the phase characteristics of seams. This study provides crucial theoretical support for the design and optimization of large-aperture exposure-tiled gratings.

https://doi.org/10.1017/hpl.2024.51 Published online by Cambridge University Press

Acknowledgements

The authors would like to thank the staff of the SG-II laser facility and the staff of the National Laboratory on High Power Lasers and Physics, Shanghai Institute of Optics and Fine Mechanics. This study was supported by the Strategic Priority Research Program of the Chinese Academy of Sciences (No. XDA25020104).

References

1. D. Ma, Y. Zhao, and L. Zeng, Sci. Rep. **7**, 926 (2017).
2. J. Zuo and X. Lin, Laser Photonics Rev. **16**, 2100741 (2022).
3. J. Guo, Z. Gao, D. Sun, X. Du, Y. Gao, and X. Liang, High Power Laser Sci. Eng. **10**, e10 (2022).
4. T. D. Ditto, Proc. SPIE **5578**, 79 (2004).
5. N. Bonod and J. Neauport, Adv. Opt. Photonics **8**, 156 (2016).
6. C. N. Danson, P. A. Brummitt, R. J. Clarke, J. L. Collier, B. Fell, A. J. Frackiewicz, S. Hancock, S. Hawkes, C. Hernandez-Gomez, P. Holligan, M. H. R. Hutchinson, A. Kidd, W. J. Lester, I. O. Musgrave, D. Neely, D. R. Neville, P. A. Norreys, D. A. Pepler, C. J. Reason, W. Shaikh, T. B. Winstone, R. W. W. Wyatt, and B. E. Wyborn, Nucl. Fusion **44**, S239 (2004).
7. J. Qiao, A. Kalb, M. J. Guardalben, G. King, D. Canning, and J. H. Kelly, Opt. Express **15**, 9562 (2007).
8. L. Wang, M. Zhang, and Y. Zhu, Opt. Precision Eng. **29**, 1759 (2021).
9. J.-W. Zhang, W. Chen, Y. Zhou, N. Xie, H. Zhou, X. Wang, F. Jing, and X.-M. Zhang, Opt. Eng. **51**, 013007 (2012).
10. L. Shi, L. Zeng, and L. Li, Opt. Express **17**, 21530 (2009).
11. M. G. Moharam and T. K. Gaylord, J. Opt. Soc. Am. **71**, 811 (1981).
12. M. G. Moharam, T. K. Gaylord, E. B. Grann, and D. A. Pommet, J. Opt. Soc. Am. A **12**, 1068 (1995).
13. J. Zhou, M. Sun, X. Liang, J. Kang, A. Guo, Q. Yang, X. Xie, J. Zhu, and Z. Lin, Chin. J. Lasers **44**, 0801007 (2017).
14. S. Mainguy, I. Tovena-Pécault, and B. Le Garrec, Proc. SPIE **5991**, 59910G (2005).
15. M. G. Moharam, T. K. Gaylord, D. A. Pommet, and E. B. Grann, J. Opt. Soc. Am. A **12**, 1077 (1995).
16. J. Li, L. Shi, Y. Ma, Y. Ran, Y. Liu, and J. Wang, Antennas Wirel. Propag. Lett. **20**, 83 (2021).
17. Q. Xu, X. Su, X. Zhang, L. Dong, L. Liu, Y. Shi, Q. Wang, M. Kang, A. Alù, S. Zhang, J. Han, and W. Zhang, Adv. Photonics **4**, 016002 (2022).
18. J. Kim, J. Seong, Y. Yang, S.-W. Moon, T. Badloe, and J. Rho, Adv. Photonics **4**, 024001 (2022).
19. S.-D. Wu and E. N. Glytsis, J. Opt. Soc. Am. A **19**, 2018 (2002).
20. Y. Chen, Y. Yang, Y. Zheng, X. Chen, K. Liu, B. He, and Q. Wu, Chin. J. Lasers **44**, 0906004 (2017).
21. D. T. Cu, T. D. Pham, V. T. H. Le, M. C. Li, H. P. Chen, and C. C. Kuo, Nanomaterials **12**, 1952 (2022).
22. Y. Han, H. Cao, F. Kong, Y. Jin, and J. Shao, High Pow Laser Sci. Eng. **11**, e60 (2023).

https://doi.org/10.1017/hpl.2024.51 Published online by Cambridge University Press